Dynamic buckling of foam stabilised composite skin

S. Rivallant [a,*], J.F. Ferrero [b], J.J. Barrau [b]

[a] IGM - SUPAERO - LMS, 10 av. E.Belin 31055 Toulouse Cedex, France
[b] IGM - LGMT - UPS, 118 Rte de Narbonne, Bât 3R1 31062 Toulouse Cedex, France

Available online 2 March 2005

Abstract

Presented in the following pages is an experimental and numerical study of dynamic local buckling of skin on foam core. Impact tests on sandwich-type structures with skins stabilized by foam demonstrated that rupture appears by debonding of skins due to a local buckling phenomenon, and that the maximum stress in the skin, obtained at rupture, grows with the increase of the loading rate of the skin. A finite element analysis allows this phenomenon to be analyzed and understood, and a mass-spring-dashpot model is proposed to model the skin debonding initiation.

Keywords: Composite; Impact; Dynamic buckling; Foam core; Composite skin; Skin debonding; Sandwich

1. Introduction

Sandwich structures are widely used in the aeronautics industry. Helicopter blades are one specific example. Indeed, in general, a helicopter blade is made of a main spar, a filler material (foam or honeycomb), and a skin covering them. One major drawback of sandwich structures is the problem of local buckling of their skins. As for the blades, normal flying conditions do not produce loads in the skins large enough to initiate buckling. However, when a blade receives a violent impact (bird, hail, etc.) the compressive load transmitted to the skins (Fig. 1) can cause them to buckle. Impact tests on blades and analyses of flight incidents particularly show partial debonding of the skins.

The phenomenon of skin debonding by local buckling under dynamic loads is still little-understood today. The problem of static local buckling has been studied for a long time, for example in the works of [1–3]. A recently-developed model even takes into account, simply but accurately, the evolution of the strain field in the core thickness [4]. Studies on buckling and the influence of loading rate have been carried out for slender beam-type structures [5] or sandwich beams, but to our knowledge no study takes the problem of local buckling into account. For these slender structures, studies usually show a clear increase in the buckling load when the loading rate increases, due to the inertia of the movement in the transverse direction. For skins covering foam or elastic medium, the phenomenon becomes more complex with the presence of transverse resistance due to the elastic environment.

By means of fine finite element analyses and good knowledge of the materials (skin and foam) and of the geometry of the skin-foam structure (initial defects), it is possible to achieve a good evaluation of the behavior of the skin in high speed dynamics, and thus of the rupture. The problem often arising with this type of structure, especially in the case of impact upon helicopter blades, is how to model the phenomenon within a global modeling of the structure. Indeed, the buckling studied here is a local phenomenon. The size of the wavelengths involved may be small compared to the dimensions of the structure. Thus, the fine modeling of the areas where

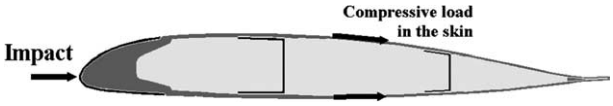

Fig. 1. Helicopter blade section.

the buckling is likely to occur means a significant increase in the size of the models and in calculation time.

This paper proposes a definition of a debonding initiation criterion under dynamic buckling, for flat skins supported by an elastic foam-type material and submitted to impact. This criterion makes it possible to produce a global modeling of the structure with reasonably-sized models.

2. Experimental study

An experimental study was completed in order to show how loading rate influences the appearing of skin debonding. The experiments consisted of impact tests on specific structures having the typical overall characteristics of a helicopter blade section.

2.1. Description of tests

The impact tests, in laboratory conditions, used a drop-weight method, with a specially-devised drop-weight apparatus. The mobile weight is connected to an accelerometer and a load cell (Fig. 2) and housed inside 2 tubes [6] (Fig. 3). The impactor weighs 990 g.

An optical speed measurement system gives the speed of the weight before and after impact. The accelerometer, by integration, gives the speed and the displacement of the impactor over time. Because the overall stiffness of the weight is greater than that of the structures tested, the displacement of the point of impact with the structure is considered equal to the displacement calculated by double integration. By measuring the force with the piezoelectric load cell, the impact load can be found.

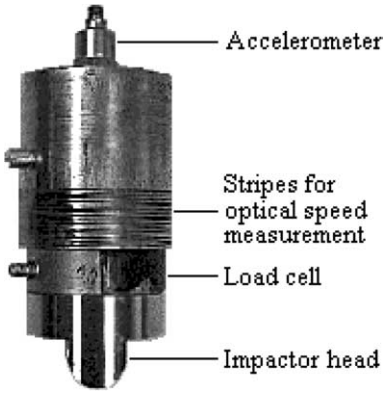

Fig. 2. Instrumentation details.

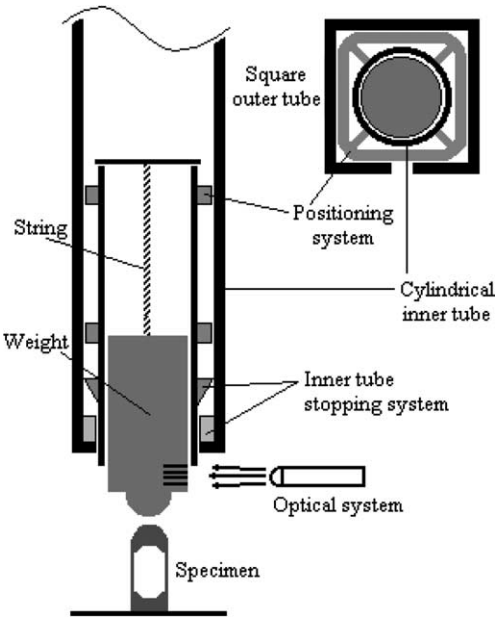

Fig. 3. Drop-weight apparatus.

The impacted specimen are thick sandwich beam structures (Fig. 4), which enable the skin to be subjected to pure compression in order to study the local buckling and the skin debonding. The specimen core is composed of manufactured polyurethane foam on which two steel ends have been bonded. The whole structure is covered with a skin of 2-ply glass epoxy fabric at 0°/90°. The theoretical skin thickness is 0.32 mm. However, because the surfaces to be bonded are imperfect and because of the manual impregnation of resin on the fabrics, the actual skin thickness is greater. This must be taken into account when calculating the bending stiffness of the skin [6]. Strain gages are bonded at the center of both skin-covered sides to measure the longitudinal strains in the skin (Fig. 4).

The shape of the steel ends is designed to transform the impact into a loading similar to a pure compressive load in the skins, and to represent globally the behavior of a blade subjected to an impact without having to take

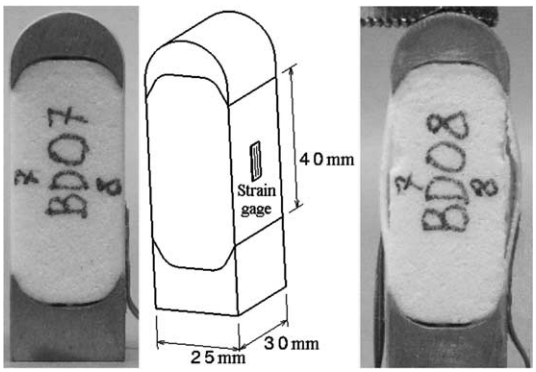

Fig. 4. Specimens before and after impact.

into account the complex problems of damage in the spar.

The speed at which the weight impacts the specimens varies from 1.5 to 4.3 m/s. The specimens also undergo static tests on an Instron machine to determine the static buckling stress in the skin.

2.2. Results

The tests show that the specimens are damaged by foam-skin debonding (Fig. 4). As in the case of debonding under static loads [6], the analysis shows that debonding is in fact due to the rupture of the foam, whose mechanical characteristics are weaker than those of the resin, at the foam-resin interface, and due also to the propagation of this rupture in the foam, along the skin. The propagation stops at the steel ends.

The static tests, done on 8 specimens, give a mean strain of 0.5% at the rupture moment, with less than 15% dispersion.

For the impact tests the weight was dropped at four speeds: 1.15, 2.3, 3.1 and 4.3 m/s. The lowest speed caused no debonding. For the 3 other speeds the strain/time graph, obtained from the strain-gages measurements, shows that when impactor speed is increased, the maximum strain observed in the skin also increases (Fig. 5). Strain is measured simultaneously on both sides of the structure, and only the mean value is plotted, after checking that the values of both measurements are consistent.

The strain rate graph has also been plotted (Fig. 6), and also shows that the strain rate in the skins increases with the speed of the impactor.

By combining both these results and adding the rupture values obtained from the static tests, it can be seen that the maximum strain (and therefore the maximum rupture stress in the skins) depends closely on the maximum strain rate of the test (and therefore the loading rate) (Fig. 7). From the static test to the 4.3 m/s impact, the maximum strain (rupture) in the skins goes from 0.5 to 0.75%, which is an increase of 50%.

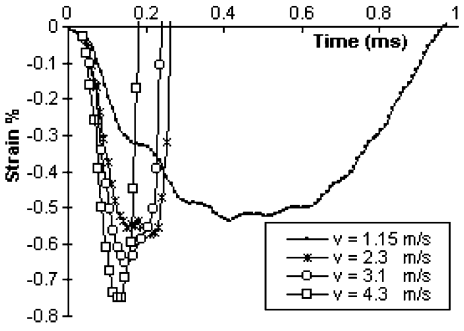

Fig. 5. Strain in the skin.

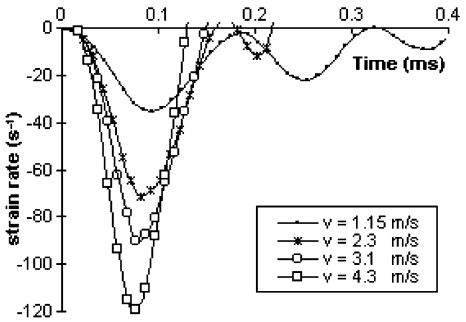

Fig. 6. Strain rate in the skin.

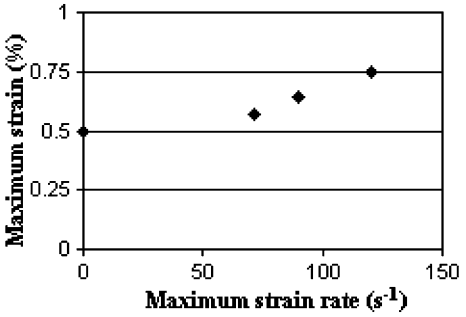

Fig. 7. Evolution of maximum strain in the skin with maximum strain rate.

3. Numerical analysis

3.1. Finite element analyses

In order to understand the process leading up to debonding, a finite element analysis has been made in high speed dynamics. It is a simplified model of skin on foam, finely meshed, incompatible with the global meshing of a structure, in order to represent correctly the evolution of stresses in the foam (Fig. 8). The debonding observed on the specimens is a 2-D phenomenon. To optimize calculation time, the finite element analysis is also in 2-D. The skin is represented by beam elements, and the foam by shell elements. The calculations were done using Radioss high speed dynamics software. The beams are classical Timoshenko-type elements [7]. The shell elements are simple bilinear Mindlin plate elements coupled with a reduced integration scheme using one integration point, with a Belytshko-type stability correction [8].

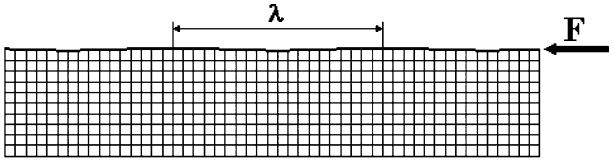

Fig. 8. Mesh with sinusoidal defect.

As is often the case when calculating non-linear stability in static, a defect has to be introduced into the geometry to cause the buckling to start. In physical terms, this defect represents a defect in the geometry or in the manufacture of the sample. The defect chosen here is an initial sinusoidal deformation of the skin, with a wavelength equal to the wavelength of the buckling deformation obtained on the same structure in static. The wavelength can be calculated from various buckling expression [1,2,4]. A realistic amplitude of around 0.1 mm is chosen, corresponding to the type of size observed in the fabrication defects.

The skin is submitted to loading by applying a load to the end of the structure in the form of a ramp.

The skin material is a glass fabric impregnated with epoxy resin. Dynamic characterization tests carried out on Hopkinson bars show the material's rupture limit to be dependent on the strain rate under compressive load, but the Young Modulus to be independent. As the debonding phenomenon studied does not lead to skin rupture before the debonding, the calculations are carried out with an elastic linear behavior law, with the static rupture strength, and a 20 000 MPa Young's modulus.

The behavior law of the foam is identified by characterization tests. Its behavior is typical of polyurethane foam [9]. The tensile law is elastic brittle, with a 0.7 MPa rupture limit. In compression, the behavior has three phases: elastic, pseudo-plastic (microbuckling of the foam cells) and a 3rd densification phase (when the cells are crushed) (Fig. 9). The compressive law is dependent on the loading rate [6]. A simplified law is applied for the finite element analysis: since the rupture appears in tension, it is considered that the foam has an isotropic brittle linear behavior, both in compression and tension, but that rupture appears only in tension.

3.2. Understanding the phenomenon

The phenomenon can be understood through the fine analysis of the evolution of the stresses inside the foam. On the model, the normal stresses in the skin and the stresses in the foam are analyzed. Finite element analyses show that when the normal load increases in the skin, a transverse displacement occurs, causing an increase in the transverse normal stress in the core. The highest level of stress is observed just beneath the skin at the points where the skin is most curved. This is true both in tension and compression, depending on the sign of the curvature. The rupture can only appear in tension. The following simplified rupture criterion is used: the rupture appears when the transverse normal stress in the foam exceeds the limit of stress in tension ($\sigma_y > \sigma_{ultimate}$). The areas of maximum stress in tension are schematized in Fig. 10 for a given moment before rupture. When the rupture criterion is reached, the debonding is initiated.

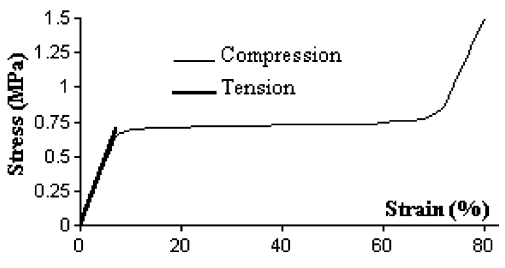

Fig. 9. Static foam behavior law.

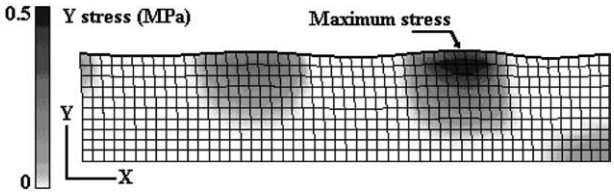

Fig. 10. Core transverse normal stress.

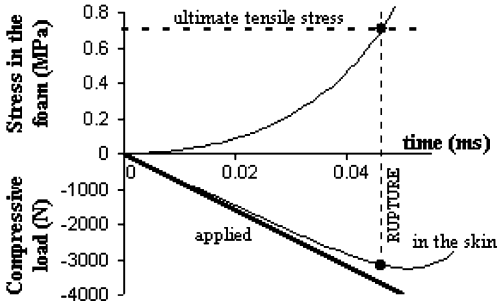

Fig. 11. Load in the skin and core transverse stress versus time.

Fig. 11 shows the parallel evolution of the compressive load in the skin and of the maximal transverse normal stress in the foam over time. The calculation is done for a loading rate of 80 N/μs. The normal load in the skin follows the imposed ramp until the transverse displacement become too great. This load is then seen to diminish. When the transverse normal stress in the foam is also plotted, it can be seen to have a nonlinear increase until reaching the rupture limit in the foam before the load in the skin decreases.

3.3. Influence of the load

To visualize the effect of the loading rate, the calculations are completed for various loading ramps. The value of the load in the skins is shown in Fig. 12. When the strain rate increases, the rupture appears earlier, whereas the maximum load in the skin before rupture increases significantly: from 1000 N in a quasi-static case, to 7500 N for a 400 N/μs ramp. When the loading rate is low, the rupture load asymptotically tends toward the static buckling value.

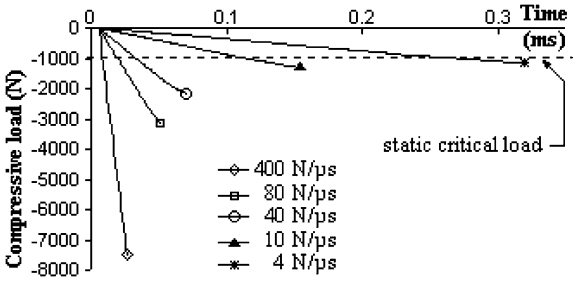

Fig. 12. Load in the skin versus time for different load rates.

Fig. 13 plots the tensile transverse stress versus the load in the skin. This graph shows that for a given initial defect, when the loading rate increases from 4 to 400 N/µs, the compressive load reached for a given tensile stress in the foam increases significantly. This is due to the inertia of the transverse movement of the skin. The result is the observed increase of rupture load with the loading rate.

Thus, the way in which the transverse displacement evolves influences the behavior of the skin and depends on the shape of the loading. However, a constant loading rate can only be considered as a coarse approximation of the loads encountered in real operating conditions, such loads usually being more complex, like those observed in the tests (Fig. 5).

To illustrate this problem, various loads were taken into account in the calculations using Radioss. Fig. 14 shows loads by ramp of 80 N/µs terminated by constant levels of varying intensity. Load in the skin versus time, and transverse stress versus load in the skin are plotted. During the first stage of the loading, using a ramp, the stress in the foam increases with the load. When the load is stabilized (constant level), the stress in the foam continues to increase until it reaches the rupture point. If the value of the load of the level is greater than the static critical value, the transverse movement initiated by the buckling can only grow greater until the rupture occurs.

Likewise, a double-ramp loading can be analyzed (Fig. 15). The first ramp is slow. It can cause a significant transverse displacement in the foam, and thus a non zero stress state. By then applying a second, faster ramp, rupture is obtained faster than if only the latter ramp had been used to start with, because far less increase in stress is now needed to reach the rupture point.

These calculations highlight the complexity of the problem. On the one hand, the load needed to cause rupture and the rupture moment greatly depend on the loading rate, but on the other hand, they depend more generally on the evolution of the load over time and also on the initial state of stresses in the foam, such as the one caused by a slow initial loading.

3.4. Influence of initial defect

Having shown that the transverse displacement of the skin is a determining factor in the subsequent behavior of the structure, the characteristic of the existing defect incorporated into the calculations is primordial. At the present stage of the research, the defect is sinusoidal, its wavelength equal to that of the deformation under static buckling. The influence of the defect's amplitude

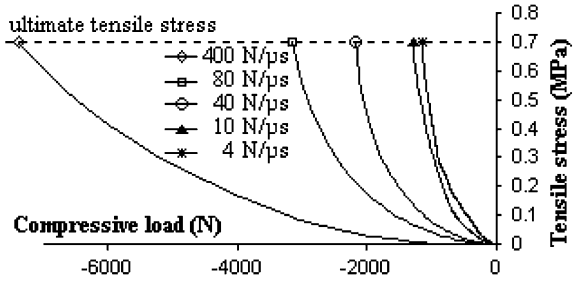

Fig. 13. Core transverse stress versus compressive load in the skin for different load rates.

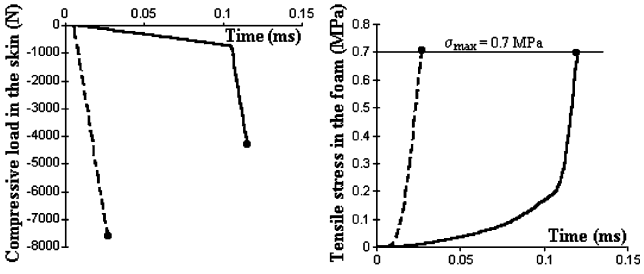

Fig. 15. Influence of loading: double ramp.

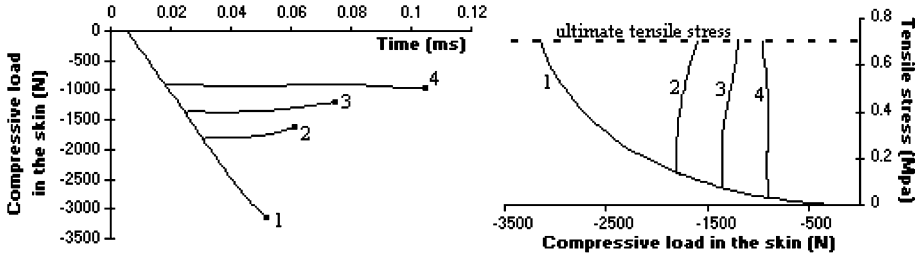

Fig. 14. Influence of loading: different levels of load for the same initial loading rate.

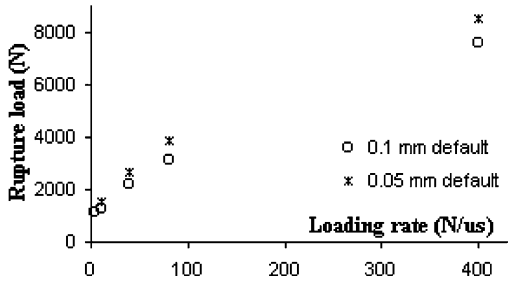

Fig. 16. Influence of initial default amplitude.

has been studied. Two amplitude are considered numerically: 0.05 and 0.1 mm. The results of these calculations (Fig. 16) show that the resistance to debonding increases when the defect diminish, as a greater transverse displacement must occur before rupture.

4. Debonding criterion

Following the conclusion drawn in the previous paragraph, the research was limited to the search for a criterion to determine the rupture load for a given defect. As seen above, a fine modeling of a structure consisting of a skin bonded on a foam core enables the rupture load and moment to be determined. This study aims to show that a simple criterion can be determined for a given skin-foam structure, making it possible to determine the rupture for any load applied to that skin, and without requiring the fine modeling of the global structure, thus reducing calculation cost.

Static studies [6] of the compression of a skin with a defect show that the amplitude of the transverse displacement depends directly on the load applied, by the intermediary of the overall stiffness of the structure (Fig. 17). The gap observed between the transverse displacement and the stress in the skin during dynamic loading can be partly explained by the inertia when the skin begins moving in the transverse direction. This observation, along with the analyses of the finite element response of the structure to dynamic loads, definitely show an analogy between the behavior of a mass-spring-dashpot system submitted to a transitory load and the response of a skin to dynamic buckling. The springs represent the overall stiffness of the structure, in static, and the masses and dashpot enable the above-mentioned inertia effects to be controlled.

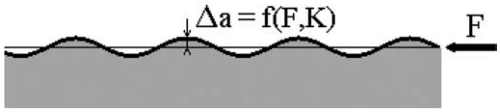

Fig. 17. Static buckling deformation.

It was therefore decided to seek the simplest possible mass-spring-dashpot model which, by identification, could simulate the response of the structure for any loading. The identification is carried out using finite element calculations, modeling only the elementary skin-foam structure submitted to a sample range of adapted dynamic loads.

It should nevertheless be noted that unlike the works of [5] and [10] on buckling of beams, our study does not aim to characterize the dynamic buckling of the skin but to determine the skin debonding by rupture in the core caused by the buckling. This is why we do not dwell on the problems of determining buckling criteria raised by [11] and [10], but we adopt a pragmatic approach by identification.

4.1. Fladyn criterion

The mass-spring-dashpot model is envisaged with a minimum number of parameters enabling the physical phenomenon to be represented. After a number of different tests, a 3-parameter model is chosen. It is shown in Fig. 18.

The parameters of the model are M, k and C by analogy with the mass, the spring stiffness and the dashpot coefficient. The maximum displacement variable x_{max} is assimilated to the maximum transverse normal stress in the foam ($\sigma_{ultimate}$). The equation to be solved is:

$$M \cdot \ddot{x} = F - C \cdot \dot{x} - k \cdot x \quad (1)$$

The calculation is done using an explicit integration scheme. When displacement reaches its maximum value x_{max}, which is equal to the rupture point in the foam, the debonding by buckling appears. The debonding moment and the value of the load in the skin are then obtained.

The parameters of the model are identified from finite element calculations. By knowing the static buckling load, the unknowns can be reduced by the expression:

$$F_c = k \cdot x_{max} \quad (2)$$

This load is obtained by the classical dynamic skin buckling formulations [1–3], or by using a model developed in the laboratory [4].

All the parameters needed can thus be determined from finite element calculations carried out with two different dynamic load cases. Further calculations (other load cases) are effectuated to ensure that the model is representative and to optimize its parameters.

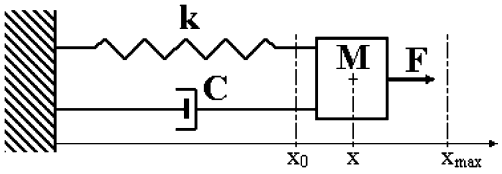

Fig. 18. Mass-spring-dashpot model.

Fig. 19 shows both the load at rupture and the rupture moment, obtained by finite element calculations and by the Fladyn criterion after determining the parameters. The different loads applied to the skin are shown in the upper graph. These loads vary in nature (different ramps, different levels, double-ramp loading) in order to validate the parameters of the model. The lower graph shows the value of the load at rupture, calculated using the Fladyn model and the finite element analyses, for comparison. For all the loads plotted, there is less than 10% difference (both for load value and debonding initiation moment), with a standard deviation of 4%.

The structure has the following characteristics:

- skin: $E_s = 20\,000$ MPa, $I_z = 0.37$ mm^4
- foam core: isotropic, $E_c = 10$ MPa, $\nu = 0.0001$, $\sigma_{max} = 0.7$ MPa en tension
- defect: wavelength $\lambda = 10$ mm, amplitude 0.1 mm
- static critical buckling load: $F_c = 1000$ N.

The values leads directly to the following values of the model parameters:

- $x_{max} = \sigma_{max} = 0.7$
- $k = 1428$

Then, by identification, the remaining parameters are:

- $M = 10^{-6}$
- $C = 0.06$

Calculations are also carried out to demonstrate that when the load in the skin is no greater than the static buckling critical value, the Fladyn criterion determines that there is no debonding of the skin.

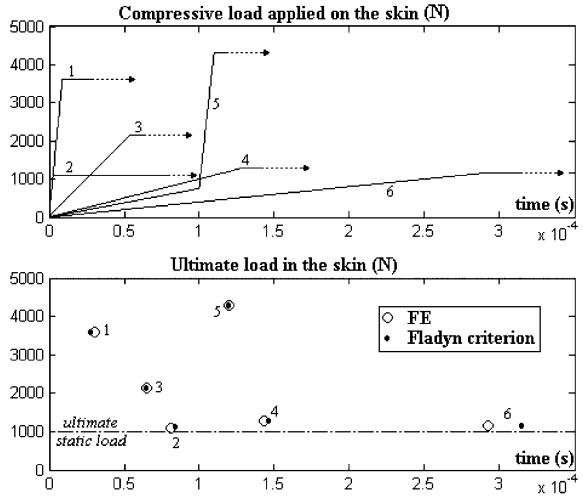

Fig. 19. Validation of Fladyn criterion parameters from different load cases.

4.2. Correlation with the tests

The Fladyn criterion is applied to the impact tests described in Section 2.1, in order to validate the method. The calculations were done on Radioss software in 2D and 3D (Fig. 20) for different mesh densities. The finite element calculations enable the load in the structures skins to be determined in relation to the speed of the drop weight. Very similar results were obtained from the 3D and 2D models. To optimize calculation time, only the 2D models are therefore used. No geometric defect is imposed on the structure, thus similar results for stress in the skin are obtained with 2D-fine and 2D-coarse mesh model, and the beginning of buckling occurs much later than in the tests, even with the 2D-fine mesh model. The Fladyn criterion must therefore be applied in both cases. The stress in the skin being similar for both types of modeling, we have chosen to proceed only with the simplified mesh, which is likely to be used in the global modeling of a structure.

The Fladyn criterion is then applied to the load values in each element of the skin to determine the ultimate load and the rupture moment. Two different defect amplitude are taken into account when determining the parameters of the Fladyn criterion: 0.05 and 0.1 mm. Fig. 21 shows the strain in the skin during the test with drop-weight speed of $v = 2.3$ m/s, and the strain measured at the gage position during finite element calculation (coarse mesh). The initiation moments, calculated by Fladyn, are plotted on each curve. The difference between the finite element curve and the tests after initiation can be put down to the fact that the debonding is not modeled with finite element. Further study is

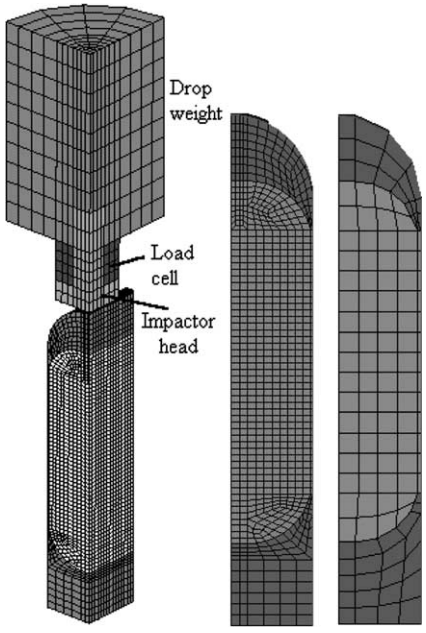

Fig. 20. Mesh of the specimen: 3D, 2D fine and 2D coarse.

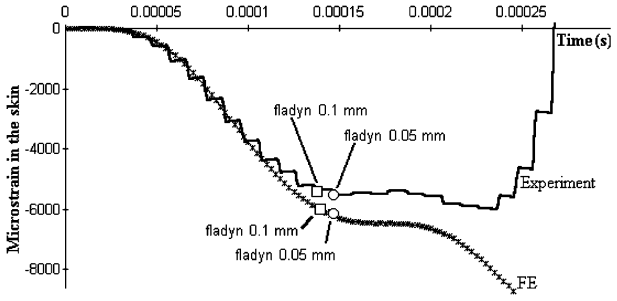

Fig. 21. Fladyn criterion applied to $v = 2.3$ m/s impact.

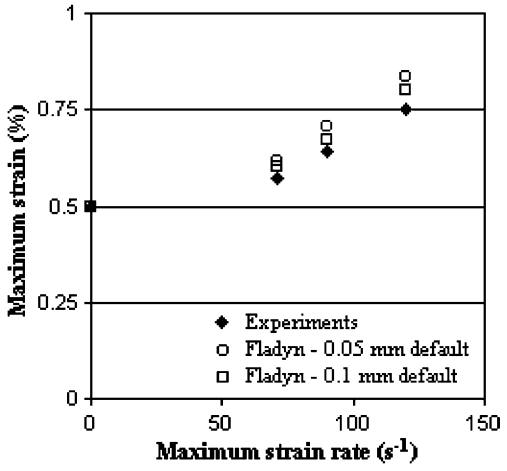

Fig. 22. Maximum strain in the skin versus maximum strain rate: experiments and numerical calculation.

already underway into the control of the evolution of the debonding, and results will be published in the near future. The loading of the skins continues, then, after determining the initiation of debonding, whereas in the tests the skin becomes unloaded after a short period of constant load.

The above calculations are completed for all the tests described in the experimental stage. Fig. 22 gives the evolution of the maximum strain in the skins with the relation to the maximum strain rate for these 3 tests and for the static tests.

Good correlation is observed between the model and the tests, which shows that the Fladyn criterion can be used as a criterion for detecting the debonding of skin on foam caused by dynamic buckling.

5. Conclusion

The Fladyn criterion is a highly useful aid in the prediction of debonding caused by dynamic buckling. From a small number of local finite element analyses, it leads to a good estimate of the load and the debonding initiation of skin on foam core structure, and for every type of compressive load. The model is now being used on structures which can be assimilated to 2D problems, and it takes into account a given initial defect in the structure. Research is underway to extend the field of application to the more complex problem of 3D structures, with the aim of applying it to the specific case of impacts on helicopter blades. Further calculations attempt to integrate the influence of defect amplitude into the Fladyn criterion by increasing the number of parameters in the mass-spring-dashpot model.

Finally, laboratory research is being done into how the debonding of skin propagates. The aim is to eventually propose a complete modeling of skin debonding, from initiation to propagation.

References

[1] Allen HG. Analysis and design of structural sandwich panels. London, UK: Pergamon Press Ltd; 1969.
[2] Hoff NJ, Mautner SE. Buckling of sandwich type panels. J Aeronaut Sci 1945;12(3):285–97.
[3] Aiello MA, Ombres L. Local buckling of sandwich panels made with laminated faces. Compos Struct 1997;38(1–4):191–201.
[4] Rivallant S. Flambement de structures composites stabilisées par une mousse. In: Proceeding of JNC13, Strasbourg, 12–14 March 2003, vol. 1, p. 243–53.
[5] Zhang Z, Taheri F. Numerical studies on dynamic pulse buckling of FRP composite laminated beams subject to an axial impact. Compos Struct 2002;56:269–77.
[6] Rivallant S. Modélisation à l'impact de pales d'hélicoptères, PhD Thesis, Supaero, France, 2003.
[7] Radioss theory manual, version 4.2, 2001.
[8] Belytschko T, Leviathan I. Physical stabilization of the 4-node shell element with one point quadrature. Comput Methods Appl Mech Eng 1994;113(3–4):321–50.
[9] Gdoutos EE, Daniel IM, Wang K-A. Failure of cellular foams under multiaxial loading. Composites 2002;Part A 33:163–76.
[10] Ari-Gur J, Elishakoff I. Dynamic instability of a transversely isotropic column subjected to a compression pulse. Comput Struct 1997;62:811–5.
[11] Hutchinson JW, Budiansky B. Dynamic buckling estimates. AIAA J 1966;4(3):525–30.